Applied Catalysis B: Environmental 325 (2023) 122302

Contents lists available at ScienceDirect

Applied Catalysis B: Environmental

journal homepage: www.elsevier.com/locate/apcatb

Waste-battery-derived multifunctional zinc catalysts for glycolysis and decolorization of polyethylene terephthalate

Yu-Wen Chiao [a,1], Weisheng Liao [a,1], Philip Anggo Krisbiantoro [a,b,c], Bor-Yih Yu [a,*], Kevin C.-W. Wu [a,b,**]

[a] Department of Chemical Engineering, National Taiwan University, Taipei 10617, Taiwan
[b] Molecular Science and Technology Program, Taiwan International Graduate Program, Academia Sinica, Taipei 11529, Taiwan
[c] International Graduate Program of Molecular Science and Technology, National Taiwan University, Taipei 10617, Taiwan

ARTICLE INFO

Keywords:
Polyethylene terephthalate
Bis(2-hydroxyethyl) terephthalate
Glycolysis
Carbon–zinc batteries
Zero-valent zinc
Dye degradation

ABSTRACT

In this study, novel and easily recyclable catalysts were prepared from waste batteries for efficient glycolysis and decolorization of polyethylene terephthalate (PET) to obtain bis(2-hydroxyethyl) terephthalate (BHET). At 190 °C and 5 h, the PET conversion and BHET yield reach 89.7 and 77.7%, respectively, which are comparable to the values obtained for the commonly used catalyst zinc acetate. Species generated from the reaction between ethylene glycol (EG) and zinc plates (e.g., Zn-glycolate, ZnO, and other metal species on zinc plates) demonstrate excellent catalytic performance. Furthermore, dye molecules released from several commercial-colored PET bottles during glycolysis can be degraded to colorless molecules using zinc plates, thereby facilitating BHET purification. The exposed zero-valent zinc from the zinc plates in EG is responsible for degrading the dye molecules. Finally, the scaled-up PET glycolysis process is conceptually designed using Aspen Plus software. The simulation results suggest that reducing the energy requirement in distillation is necessary for further improvement.

1. Introduction

Owing to critical environmental issues resulting from the rapid production of PET waste, PET recycling has recently attracted considerable attention. Currently, the PET recycling industry uses physical recycling to process colorless PET bottles into recycled PET (r-PET). However, physical recycling cannot easily process colored PET bottles and textiles, which are therefore mainly landfilled or incinerated. Chemical recycling has emerged as an active research area in recent years to solve these problems. Glycolysis is one of the most promising chemical recycling methods because of the mild reaction conditions, low volatility of ethylene glycol (EG), and the possibility of repolymerizing the product bis(2-hydroxyethyl) terephthalate (BHET) into PET in fewer steps than those required for other monomers.

As PET glycolysis is known to be a sluggish reaction, homogeneous or heterogeneous catalysts are indispensable. Homogeneous catalysts active for PET glycolysis include metal acetates (Zn, Mn, Co, and Pb) [1,2], sodium carbonate [3], 1,5,7-triazabicyclo[4.4.0]dec-5-ene [4], ionic liquids [5], and deep eutectic solvents [6]. Although these catalysts have been reported to exhibit high catalytic performances, they are difficult to separate from the medium. Therefore, heterogeneous catalysts are preferred. Heterogeneous catalysts such as metal oxides (e.g., ZnO or CeO_2) [7,8], metal–organic frameworks (e.g., ZIF-8 or MAF-6) [9,10], Mg–Al hydrotalcite [11], and metal ferrites (e.g., $CoFe_2O_4$) [12] can help resolve the separation problem, but exhibit decreased catalytic activity. Consequently, developing cost-effective and easily recyclable catalysts with high catalytic activity is critical for PET glycolysis.

In this study, we evaluate the use of waste-battery-derived centimeter-sized and commercially-available zinc plates as easily recyclable and highly active catalysts for PET glycolysis. While these zinc plates are active for PET glycolysis with the activity comparable to that of the commonly employed catalyst zinc acetate, they can be easily separated from the glycolysis products. X-ray diffraction spectroscopy (XRD) and X-ray photoelectron spectroscopy (XPS) were used to characterize the

* Correspondence to: No. 1, Sec. 4, Roosevelt Road, Taipei 10617, Taiwan.
** Corresponding author at: Department of Chemical Engineering, National Taiwan University, Taipei 10617, Taiwan.
E-mail addresses: boryihyu@ntu.edu.tw (B.-Y. Yu), kevinwu@ntu.edu.tw (K.C.-W. Wu).
[1] Yu-Wen Chiao and Weisheng Liao contributed equally to this work.

https://doi.org/10.1016/j.apcatb.2022.122302
Received 27 September 2022; Received in revised form 14 December 2022; Accepted 16 December 2022
Available online 20 December 2022

composition of the zinc plate before the reaction and the species generated on the plates during the reaction. The effects of the catalyst amount, temperature, and time were investigated to determine the optimum conditions, kinetic data, and apparent activation energy (E_a) for the system. Moreover, several commercial-colored PET bottles were subjected to glycolysis to examine the degradation of dye molecules released from these colored PET bottles by zinc plates in EG. While the mechanisms for PET glycolysis and dye degradation by zinc plates are proposed, the feasibility of using zinc plates for industrial-scale applications is demonstrated through an Aspen Plus simulation.

2. Experimental

PET pellets (2.0 × 2.5 × 2.5 mm) with an intrinsic viscosity of 0.80 ± 0.02 dL/g were provided by LIBOLON (Taiwan). Colorless and colored PET bottles were obtained from Coca-Cola (colorless), Schweppes sparkling water (blue), TAIYEN sparkling water (light blue), mini-Oligo water (green), and Sprite (green). Zinc plates were obtained from waste carbon–zinc batteries or local companies. Ethylene glycol (EG, 99.5%) and tetrahydrofuran (THF, HPLC grade) were purchased from Acros. Zinc oxide (ZnO, ≥99%), dimethyl sulfoxide-d_6 (DMSO-d_6, 99.9 atom %), and azobenzene (98%) were provided by Sigma–Aldrich. Zinc acetate dihydrate and antimony(III) oxide (Sb_2O_3, 99%) were from Alfa Aesar. Nitric acid (≥ 65%) was purchased from Fluka; bis(2-hydroxyethyl) terephthalate (BHET, 97%) and anthraquinone were obtained from TCI.

The zinc electrode was dismantled from the waste battery and cut into small zinc plates (0.5 × 0.5 cm), which were used as catalysts for the PET glycolysis reaction after simple cleaning and drying (Fig. 1S). The zinc plates were characterized using XRD (Rigaku SmartLab SE), XPS (Thermo Scientific, Theta Probe), and field-emission scanning electron microscope/energy dispersive spectroscopy (FE-SEM/EDS; FEI, Nova™ NanoSEM 230). The detailed experimental procedure for PET glycolysis and the product is described in the Supporting Information. Typically, PET pellets were added to pre-heated EG in a round flask, and catalysts were added to initiate the glycolysis reaction. After a predetermined reaction time, the solution was cooled, and deionized water was added to the solution under vigorous stirring to separate the undepolymerized PET and high-molecular-weight oligomers. Subsequently, BHET was obtained through crystallization at a low temperature (4 °C), followed by filtration. The purity of the as-produced BHET was analyzed using differential scanning calorimetry (DSC; TA Instruments, SDT 650), gas chromatography–mass spectrometry (GC/MS; Agilent 6890/5975), and ^{1}H nuclear magnetic resonance spectroscopy (^{1}H NMR; BRUKER, AVIII-500 MHz FT NMR). The zinc content in EG and in BHET after zinc-plate-catalyzed glycolysis was determined using inductively coupled plasma–optical emission spectrometry (ICP-OES; Thermo Fisher Scientific iCAP PRO). The size of the species generated between the zinc plate and EG at elevated temperatures was analyzed using dynamic light scattering (DLS; Malvern, Zetasizer Nano). Colored PET bottles were analyzed using ultraviolet–visible (UV–Vis) spectrophotometry (Jasco V-670).

3. Results and discussion

3.1. Characterization of zinc plates

Fig. 1 shows the XRD spectra of the waste-battery-derived and commercially available zinc plates. Both zinc plates possess typical diffraction patterns of metallic zinc and ZnO. The diffraction line at 36.22° is attributed to the (1 0 1) plane of ZnO [13,14], whereas the diffraction patterns at 36.26, 38.84, 43.05, 54.18, 69.96, and 76.92° can be assigned to the (0 0 2), (1 0 0), (1 0 1), (1 0 2), (1 0 3), and (0 0 4) planes of metallic zinc, respectively [15–17]. This is expected because metallic zinc can be easily oxidized to form ZnO when exposed to air [18]. Furthermore, the intensity of ZnO in zinc plates from waste

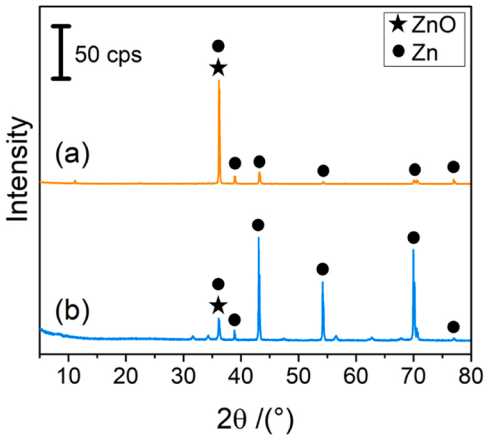

Fig. 1. XRD spectra of (a) zinc plate from waste carbon–zinc battery and (b) commercial zinc plate.

batteries is higher than that in commercial zinc plates, thus indicating the relatively high ZnO content of the battery-derived zinc plate.

Because heterogeneous catalysis occurs on the surface of the catalysts, the species involved in the reaction must be examined. Thus, XPS analysis is used to determine the surface information and chemical state of the zinc plates (Fig. 2). As shown in Fig. 2a, C 1s exhibits only one peak (284.6 eV) attributed to adventitious carbon, which is a thin carbonaceous material on the surface of samples that are exposed to air [19,20]. The absence of a peak attributed to C from carbonate species at 290.4 eV indicates that zinc carbonate is not observed on the surface of the zinc plates [21]. For Zn 2p, as shown in Fig. 2b, only one peak can be assigned to the superposition of Zn^{2+} and Zn^0, because both Zn^{2+} and Zn^0 possess similar binding energies at approximately 1022.55 and 1019.35 eV [15], respectively. Therefore, both Zn^{2+} and Zn^0 are present on the surface of the zinc plate. For O 1s, as shown in Fig. 2c, the peak at approximately 531 eV can be attributed to the binding energies of –Zn–O– (530.0 eV) and –Zn–OH (531.8 eV) [21], implying the existence of –Zn–O– and –Zn–OH on the surface of the zinc plates. Because the electrolyte of carbon–zinc batteries typically contains ammonium chloride or zinc chloride, XPS analysis of chlorine was performed. As shown in Fig. 2d, the absence of a Cl 2p peak indicates that Cl is not present on the surface of the zinc plate. Based on these characterizations, the zinc plates used in this study contain ZnO and metallic zinc with small amounts of adventitious carbon on their surfaces. The major components of ZnO are –Zn–O– and –Zn–OH.

3.2. PET glycolysis via zinc plates

In this study, the catalytic performance of waste-battery-derived zinc plates and commercial zinc plates for PET glycolysis was initially evaluated at 180 °C for a prolonged duration. Both zinc plates demonstrate excellent catalytic activity toward PET glycolysis, as indicated by the disappearance of PET pellets. Moreover, the analysis of glycolysis products through DSC, GC/MS, and ^{1}H NMR reveals that the products comprise high-purity BHET (Fig. 2S–4S). As both waste-battery-derived and commercial zinc plates demonstrate different peak intensities in XRD (Fig. 1), they may have different catalytic activities. Thus, the catalytic activities of both catalysts were further compared. The surface areas of both catalysts were kept constant in both experiments, as the surface area of zinc plates, instead of the weight, should determine the catalytic activity for PET glycolysis. As shown in Fig. 5S, the waste-battery-derived and commercial zinc plates present similar PET conversions, clearly indicating that both catalysts possess similar catalytic activity. Therefore, commercial zinc plates were used as the catalyst for subsequent studies to determine suitable operating conditions.

The effects of catalyst loading, reaction temperature, and residence

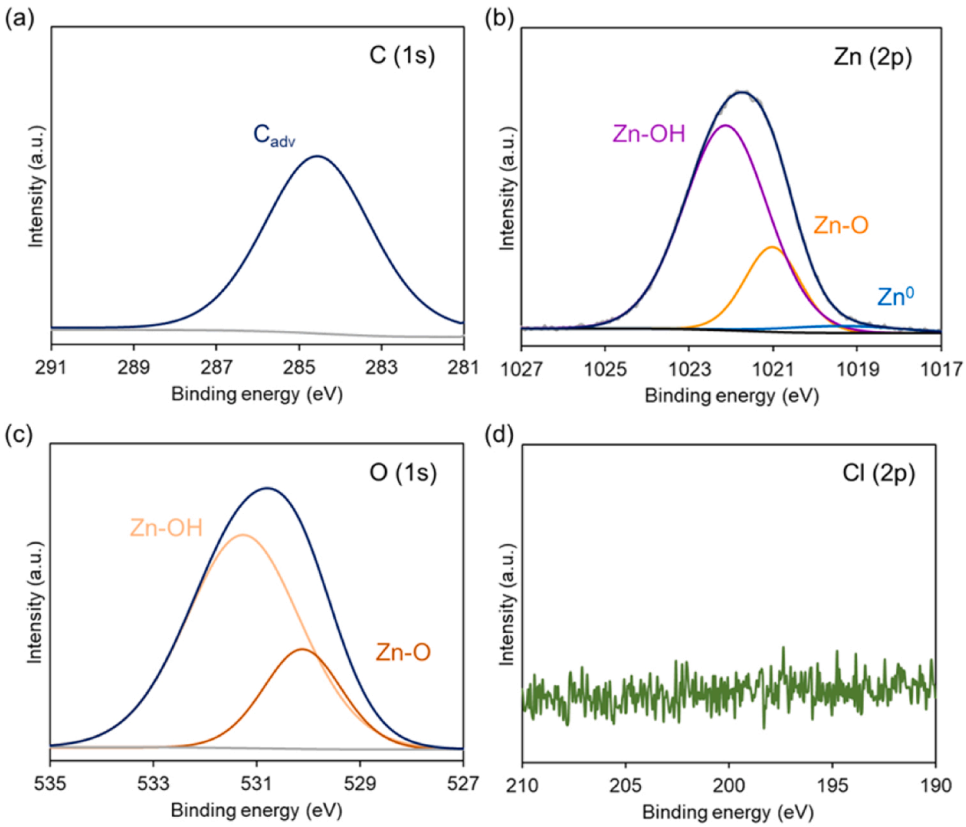

Fig. 2. XPS spectra of zinc plates for (a) C 1s, (b) Zn 2p, (c) O 1s, and (d) Cl 2p.

time on the reaction performance (i.e., PET conversion and BHET yield) are shown in Fig. 3. Each experiment was conducted using 5 g of the PET sample and 30 g of EG [10]. Fig. 3a shows the influence of the catalyst loading. Accordingly, the PET conversion steadily increases under increased catalyst loading (i.e., 78.4% under 0.5 g of catalyst; 92.4% under 3 g of catalyst). The high reactivity is comparable to (or even better than) that of zinc acetate, which has been extensively used in the industry [22]. However, the yield of BHET reaches a maximum (~72.7%) when using 2 g of catalyst. This indicates the potential repolymerization of BHET into dimers (i.e., chemical equilibrium). Fig. 3b shows the effect of temperature on PET glycolysis over zinc plates. At temperatures below 170 °C, PET is marginally converted (i.e., < 3%). However, both PET conversion and BHET yield significantly increase to 31.6 and 23.4% at 180 °C and 86.6 and 72.7% at 190 °C, respectively. Fig. 3c shows the effect of residence time on the reaction. At $t < 2$ h, the PET conversion is considerably slow owing to the "induction time," specifically, the time at which the possibility of EG reacting with the chain ends of PET is low [23,24]. The induction time can be shortened by increasing the temperature or decreasing the size of PET [3]. The PET conversion is only ~20% with negligible BHET yield at 2 h, whereas the PET conversion and BHET yield significantly increase between 2 and 5 h. At 5 h, the conversion reaches a maximum and then decreases. When glycolysis is initiated, EG demonstrates an increased probability of contacting and reacting with the S_0 sites of PET and the carbonyl groups in the middle of the PET chains (Fig. 6S). The cleavage of the S_0 sites produces two PET oligomers with low molecular weights. Most PET oligomers generated at the beginning of the glycolysis reaction are insoluble in EG and thus should not contribute to the decrease in the mass of the polymer when weighing to determine the PET conversion. However, when attacked by EG, this cleavage generates additional S_1 sites that produce the target product, BHET. As glycolysis proceeds, additional PET oligomers with decreasing molecular weights become soluble in EG, and S_1 sites are further created. Consequently, the conversion of PET and yield of BHET increase significantly [23]. In summary, the optimized glycolysis conditions are: 5 g of PET pellets, 30 g of EG, 2 g of catalyst, 190 °C, and reaction time of 5 h under an atmosphere with a PET conversion and BHET yield of 89.7 and 77.7%, respectively.

PET glycolysis can be assumed to follow pseudo-first-order reaction kinetics (Eq. 1), because EG is used in excess in the reaction [25–27]. Kinetic data for PET glycolysis via the zinc plate are summarized in Table 1. As expressed in Eq. 1, k is the rate constant of the reaction, and [PET] is the concentration of PET at time *t*. [PET] can be calculated using Eq. 2, where *X* is the conversion of PET, and $[PET]_0$ is the initial concentration of PET at $t = 0$. Combining Eqs. 1 and 2 results in Eq. 3, which can be further integrated with time to obtain Eq. 4. Based on the linear fitting plot of the first-order kinetic model presented in Fig. 4, the rate constants at different temperatures can be obtained from the slopes of each fitting line. The rate constants at 180, 190, and 195 °C are 0.30, 0.71, and 1.63 h^{-1}, respectively. The activation energy (E_a) for this reaction is obtained by applying these rate constants to the Arrhenius equation (Eq. 5). The calculated E_a is 189.7 kJ/mol, which is comparable to those reported previously, for example, MAF-6 (197.3 kJ/mol) [10] and sodium carbonate (185 kJ/mol), [3] but higher than those in some other studies wherein E_a is typically lower than 100 kJ/mol [28–30]. The apparent activation energy was measured for a heterogeneous catalytic system and could be considerably influenced by the reaction environment, including the particle size, pore size, diffusion, adsorption, and heat transfer properties of both reactants and catalysts.

$$\frac{d[\mathrm{PET}]}{dt} = -k[\mathrm{PET}] \tag{1}$$

$$[\mathrm{PET}] = [\mathrm{PET}]_0(1-X) \tag{2}$$

$$\frac{dX}{dt} = -k(1-X) \tag{3}$$

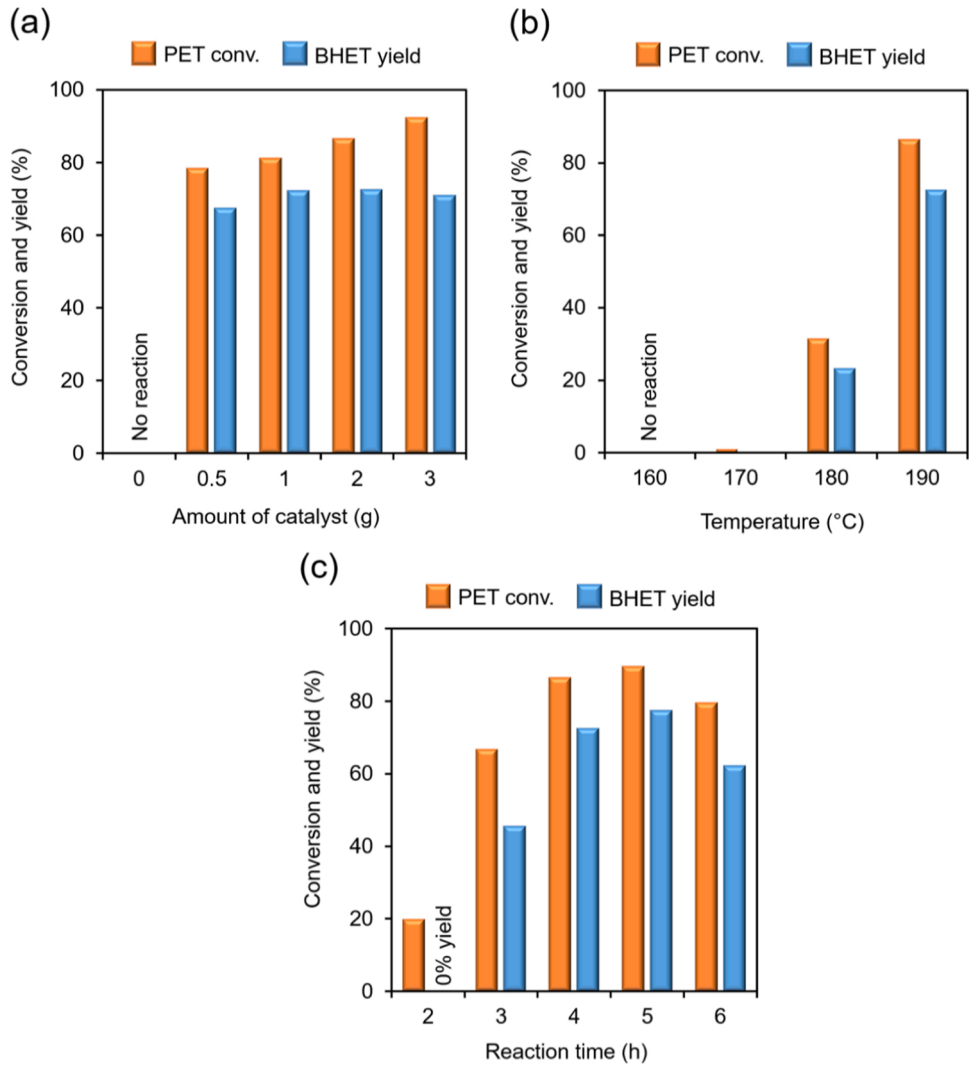

Fig. 3. Effects of (a) catalyst amount (PET, 5 g; EG, 30 g; temperature, 190 °C; and reaction time, 5 h), (b) reaction temperature (PET, 5 g; EG, 30 g; zinc plates, 2 g; and reaction time, 5 h), and (c) reaction time (PET, 5 g; EG, 30 g; zinc plates, 2 g; and reaction temperature, 190 °C) on PET glycolysis over zinc plates.

Table 1
Kinetic data for PET glycolysis over zinc plates.

Temperature (°C)	Rate constant, k (h^{-1})	Linear correlation coefficient, R^2	Activation energy, E_a (kJ/mol)	Linear correlation coefficient, R^2
180	0.30	0.9958	189.7	0.9616
190	0.71	0.9543		
195	1.63	0.9738		

$$ln\left(\frac{1}{1-X}\right) = -kt \quad (4)$$

$$lnk = lnA - \frac{E_a}{RT} \quad (5)$$

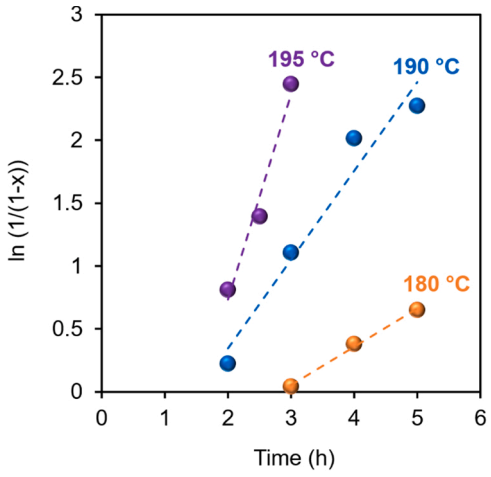

Fig. 4. Linear fitting plot of the first-order kinetic model for PET glycolysis at different temperatures. Reaction conditions: PET, 5 g; EG, 30 g; and zinc plates, 2 g.

3.3. Proposed glycolysis mechanism via zinc plates

The reaction mechanism using the zinc plates is comprehensively discussed in this section. The solution remained reactive even if the zinc plates were removed as the reaction proceeded. Hence, we speculate that other active species are formed from the reaction between the zinc plates and EG during the reaction. In a separate experiment in the absence of PET, the species formed from the reaction of the zinc plates

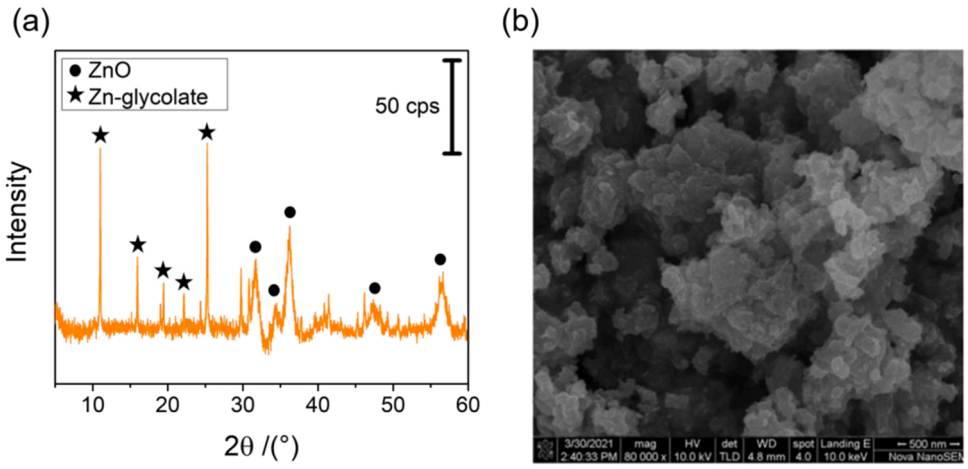

Fig. 5. (a) XRD spectrum and (b) SEM image of the generated species between zinc plates and EG at 180 °C.

and EG were collected and subsequently analyzed using XRD. The XRD pattern reveals that the species is a mixture of Zn-glycolate and ZnO (Fig. 5a). Zinc precursors in EG at elevated temperatures (>150 °C) can produce Zn-glycolate [31–33], and if a small amount of water is present in EG, Zn-glycolate is partially transformed into ZnO [31]. According to the XRD and XPS analyses shown in Figs. 1 and 2, respectively, the zinc plates are zero-valent zinc with bivalent zinc oxides. In our system, EG probably reacts with bivalent zinc ions to produce Zn-glycolate, as shown in Eq. 6. Some Zn-glycolate reacts with water to produce ZnO and EG, as shown in Eq. 7. Moreover, water is possibly obtained from reactions between ZnO and EG. Based on the SEM images, products containing Zn-glycolate and ZnO display similar morphologies to those reported in the literature [31], and the size is approximately in micrometers, as shown in Fig. 5b. These micro-sized Zn-glycolate and ZnO mixtures can catalyze PET glycolysis.Fig. 6.

$$Zn^{2+} + HO\text{-}CH_2CH_2\text{-}OH \rightarrow Zn(OCH_2CH_2O) + 2\ H^+ \quad (6)$$

$$Zn(OCH_2CH_2O) + H_2O \rightarrow ZnO + HO\text{-}CH_2CH_2\text{-}OH \quad (7)$$

The reaction between the antimony species in PET and zero-valent zinc can be considered another possible source of zinc-based catalysts. At T > 150 °C, antimony trioxide (Sb_2O_3), a catalyst for condensation reaction that remains in the structure of PET during the PET polymerization manufacturing process [34,35], is released during PET glycolysis and reacts with EG to form Sb-glycolate [$Sb_2(OCH_2CH_2O)_3$] (Eq. 8) [36, 37]. Owing to the strong reducing ability of metallic zinc (redox potential = −0.762 eV) [38], antimony in Sb-glycolate is reduced upon contact with zero-valent zinc. Reduced antimony metal is deposited on the surface of the zinc plates (Eq. 9), thus turning the zinc plates black, as shown in Fig. 7S. The EDS results of the zinc plates before and after PET glycolysis validate the existence of antimony on the surface of the zinc plate (Fig. 8S). To further confirm the chemical states of antimony, the XPS spectra of the zinc plates after PET glycolysis are obtained, showing broad Sb 3d peaks (Fig. 6), These peaks consist of Sb_2O_3 and Sb_2O_5, which are native antimony oxides formed on the surface of antimony when exposed to air. The two peaks at approximately 528 and 537 eV correspond to Sb^0, which confirms the deposition of antimony on the surface of the zinc plates [39,40]. The oxidizing zinc and liberated glycolate from Sb-glycolate combine to form Zn-glycolate when antimony is reduced by zero-valent zinc, as shown in Eq. 9, thus contributing to glycolysis. Both species may catalyze PET glycolysis. Scheme 1 summarizes the generation of plausible catalysts in PET glycolysis via zinc plates, including Zn-glycolate, ZnO, the antimony species deposited on the surface of the zinc plates, and the zinc plate itself.

$$Sb_2O_{3\ (from\ PET)} + 3HO\text{-}CH_2CH_2\text{-}OH \rightarrow Sb_2(OCH_2CH_2O)_3 + 3\ H_2O \quad (8)$$

$$3Zn^0 + Sb_2(OCH_2CH_2O)_3 \rightarrow 3Zn(OCH_2CH_2O) + 2Sb^0_{(on\ zinc\ metal\ surface)} \quad (9)$$

To understand the catalytic activity of Zn-glycolate and ZnO in EG and the antimony species on the surface of the zinc plates, a series of

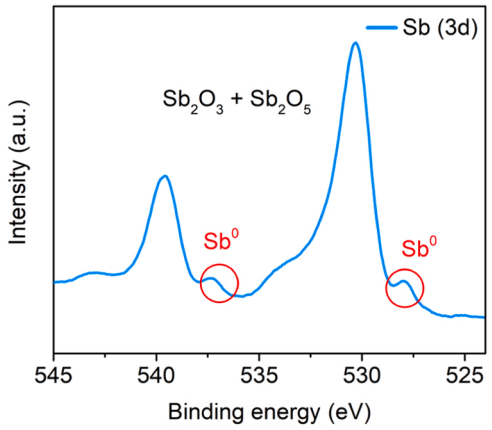

Fig. 6. XPS spectrum of zinc plates after PET glycolysis for Sb (3d). Reaction conditions for the glycolysis: PET, 5 g; EG, 30 g; zinc plate, 2 g; 190 °C; and reaction time, 5 h.

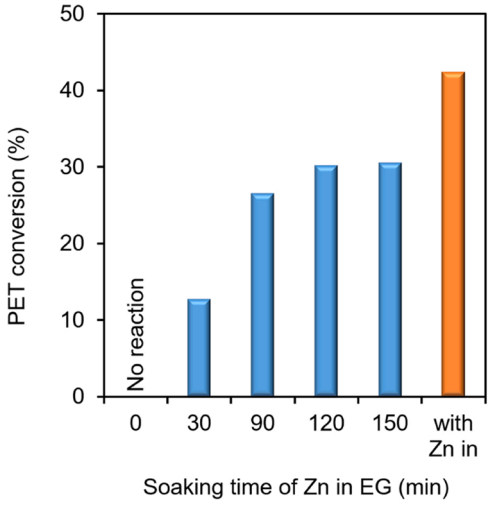

Fig. 7. PET conversion with different soaking times of zinc in EG. Reaction conditions: PET, 5 g; EG, 30 g; temperature, 190 °C; and reaction time, 2.5 h.

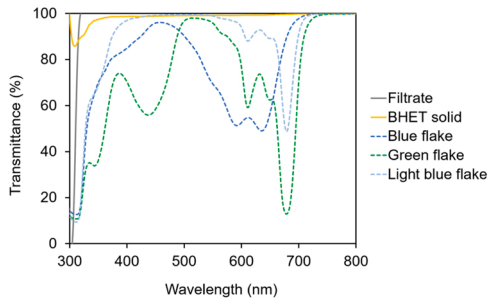

Fig. 8. UV–Vis spectra of the resulting filtrate and BHET after crystallization for glycolysis of mixed colored PET flakes.

experiments was conducted considering the following procedure: (a) the zinc plates were soaked in EG at 190 °C for different soaking times, (b) the zinc plates were withdrawn, and (c) PET glycolysis was performed with this EG solution containing Zn-glycolate and ZnO. As indicated by the blue bars in Fig. 7, Zn-glycolate and ZnO evidently influence PET glycolysis. With a soaking time of 30 min, the PET conversion is only 12.8%. However, increasing the soaking time increases the PET conversion, implying that additional Zn-glycolate and ZnO are generated. With a soaking time of approximately 120 min, the maximum conversion of PET (30.2%) is attained, indicating that the highest amounts of Zn-glycolate and ZnO are produced. The conversion of PET glycolysis in the presence of zinc plates is 42.4% (yellow bar in Fig. 7), which is higher than that in the absence of the zinc plates (blue bar). The experiments involving the zinc plates exhibit better catalytic activity than those in which the zinc plates are removed. This indicates the presence

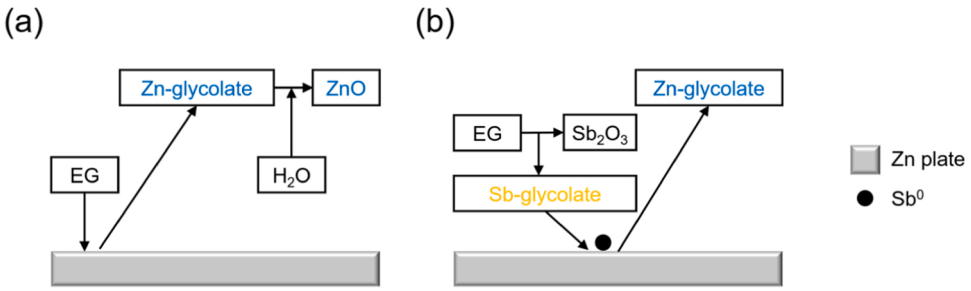

Scheme 1. (a) The generation of Zn-glycolate and ZnO from the reaction between EG and Zn plate and (b) the formation of Zn-glycolate via the interaction between Sb-glycolate and Zn plate.

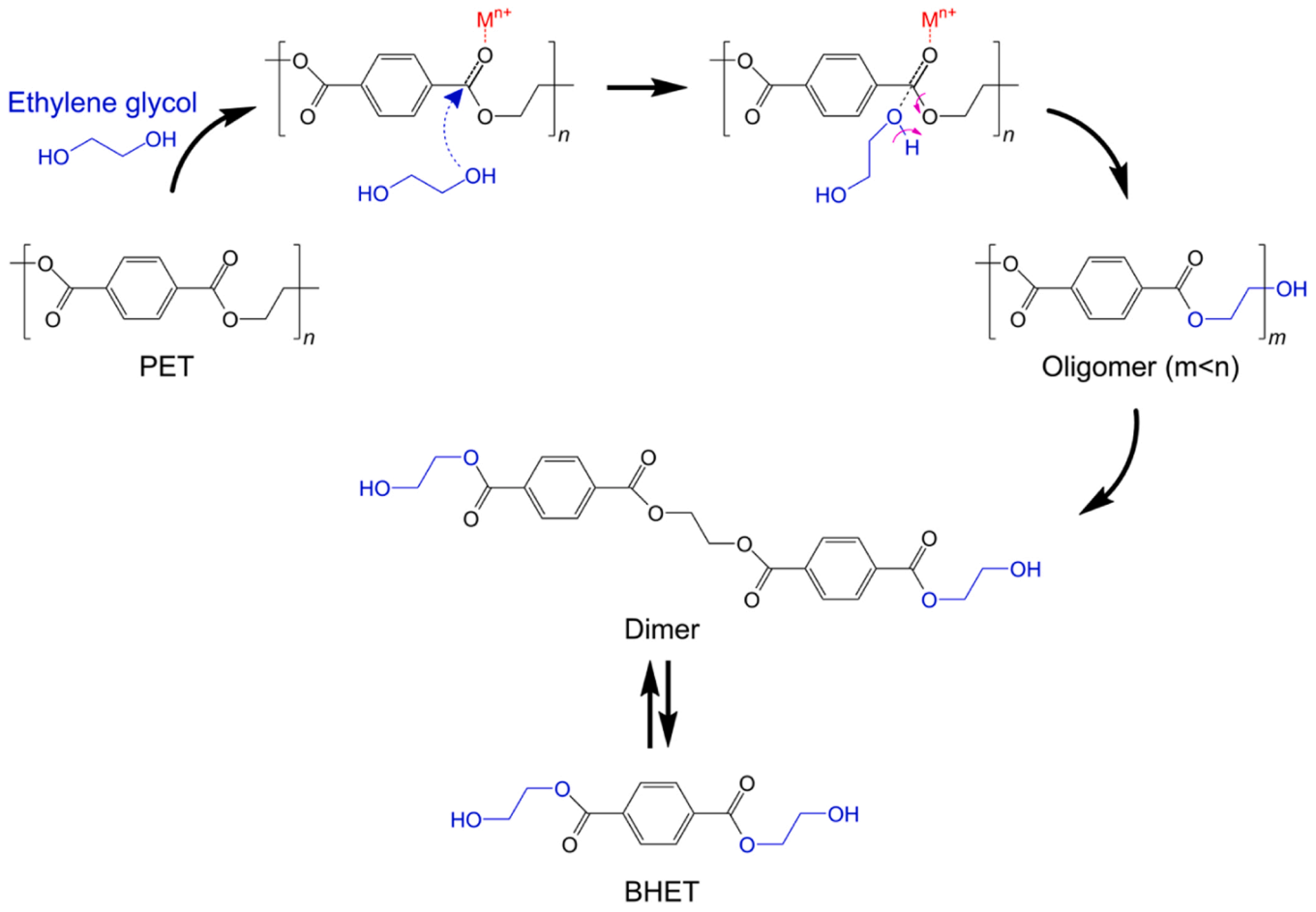

Scheme 2. Proposed mechanism of PET glycolysis over the catalysts considered in this study.

of the formed antimony species on the surface of the zinc plate and the zinc plate itself, which facilitates catalytic activity toward PET glycolysis. Furthermore, because the resultant Zn-glycolate and ZnO are in micrometers, according to the SEM image (Fig. 5b), they are readily suspended in EG and enhance the chance of interaction with PET for glycolysis. The abovementioned findings for the possible catalysts support the favorable performance of centimeter-sized zinc plates, which is comparable to that of zinc acetate. Scheme 2 shows the proposed mechanism of the PET glycolysis reaction over zinc plates. The lone electron pair of the carboxyl oxygen in the ester bond of PET is attracted by metal ions from the catalyst sources, including Zn-glycolate, ZnO, and antimony species, thus enhancing the electronegativity of carboxyl oxygen. This facilitates the attack of EG on the carbon in the ester bond of PET, and the bond is broken. Subsequently, oligomers and dimers are produced with the repeated breakage of the ester bonds of PET. Finally, monomer BHET is obtained.

3.4. Catalyst reusability

Catalyst recycling is essential for sustainable industrial application. Therefore, several catalyst recycling experiments were performed to examine the feasibility of reusing the zinc plates. Each glycolysis reaction was catalyzed using the same zinc plates under the optimized reaction conditions. After each reaction, the zinc plates were extracted with a tweezer, rinsed with water, dried overnight at 60 °C, and directly reused in the subsequent reaction. As presented in Fig. 9S, with a slight decrease in PET conversion and BHET yield, the catalytic performance is retained to obtain 70.8% of BHET yield after five runs, implying that zinc plates are still effective for glycolysis. The zinc plates demonstrate good reusability because zinc can be oxidized rapidly after the plates are dried and exposed to air, thus forming new zinc oxides. Therefore, the zinc plates can be reactivated and reused several times. The catalysts Zn-glycolate and ZnO, which are generated between the zinc plate and EG, must be separated from EG after glycolysis, because their presence in EG affects the crystallization step of BHET and its purity. Particularly, the Zn-glycolate and ZnO catalysts separated from the reaction solution can be reused for the subsequent glycolysis reaction. Therefore, the amount of Zn-glycolate and ZnO remaining in the reaction solution and BHET must be determined. The SEM image (Fig. 5b) shows that the size of the generated Zn-glycolate and ZnO mixture is between 1 and 10 μm. However, this size range cannot represent the actual size range in EG. DLS analysis was used to investigate the particle size distribution of Zn-glycolate and ZnO in EG. Four samples were prepared by reacting different weights of zinc plates with EG. Detailed DLS results are shown in Fig. 10S. According to the DLS results, the particle size of the Zn-glycolate and ZnO mixture in EG is above 100 nm in 3–6 min after the reaction. These particles can be simply removed by microfiltration, which inhibits the passage of solids with particle sizes bigger than 0.1 μm [41,42]. After PET glycolysis, the zinc plates were removed, and spent EG was filtered through a 0.22 μm nylon syringe filter to simulate microfiltration. The zinc content remaining in the reaction solution and the monomer product, BHET, produced from the crystallization step, were analyzed using ICP-OES; the content of zinc ions remaining in 30 g of EG is < 0.01 wt%. Additionally, only a trace amount of zinc ions is retained in the product BHET, that is, approximately < 0.01 wt% of zinc ions per gram of BHET. Furthermore, metal salt catalysts consistently produce the corresponding anions in EG (e.g., zinc acetate or sodium carbonate), which are difficult to remove and may contaminate BHET. In the present system, the only anion generated during glycolysis is glycolate, as shown in Eqs. 6–9, which benefits glycolysis and does not contaminate BHET.

3.5. Glycolysis of colored PET bottles via zinc plates in EG

Based on the catalyst characterization in Section 3.1, the zinc plates contain both oxidizing zinc and metallic zinc, that is, zero-valent zinc. Zero-valent zinc is a strong reducing agent and is commonly used as a dye degradation agent in acidic aqueous solutions for environmental research [43]. Therefore, we speculate that the exposed zero-valent zinc in our system during glycolysis can be used as a reducing agent for degrading the dyes released from colored PET bottles. Consequently, colored PET bottle flakes obtained from local convenience stores were subjected to glycolysis using zinc plates. The UV–Vis spectra of these colored PET flakes between 300 and 800 nm are shown in Fig. 11S, with intense transmission peaks in the visible wavelength range. After glycolysis, the transmission peaks in the visible wavelength range almost disappear (Fig. 8), even for the filtrate and BHET, thus indicating that these dye molecules are degraded into colorless molecules by the zinc plates in EG. Dye degradation is not observed when zinc acetate or ZnO are used as catalysts for blue PET flake glycolysis (Fig. 12S), as indicated by the blue color of the EG solution and BHET. The UV–Vis absorption spectra of the EG solution during glycolysis using the three catalysts are shown in Fig. 13S. The UV–Vis spectrum of the blue dye demonstrates a blue shift only when zinc plates are used as the catalysts. The blue shift implies that the conjugated structure of the blue dye may be eliminated.

Disperse dyes are the primary dye materials used for PET colorization. Two major chromophores in disperse dyes are the most used azo and anthraquinone groups [44–46]. In colored PET bottle tests, dyes released from these bottles may comprise azo groups and/or anthraquinone groups. Therefore, two model compounds, namely, azobenzene and anthraquinone, were used to determine the possibility of their

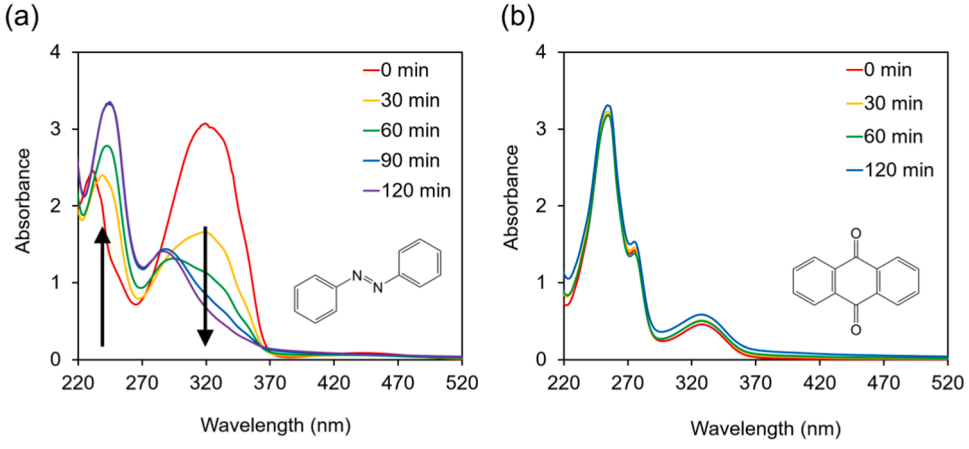

Fig. 9. UV–Vis spectra of model compounds of disperse dyes, (a) azobenzene and (b) anthraquinone, after degradation via zinc plates in EG. Reaction conditions: Model compounds, 5–10 mg; EG, 10 mL; zinc plates, 1 g; temperature, 190 °C.

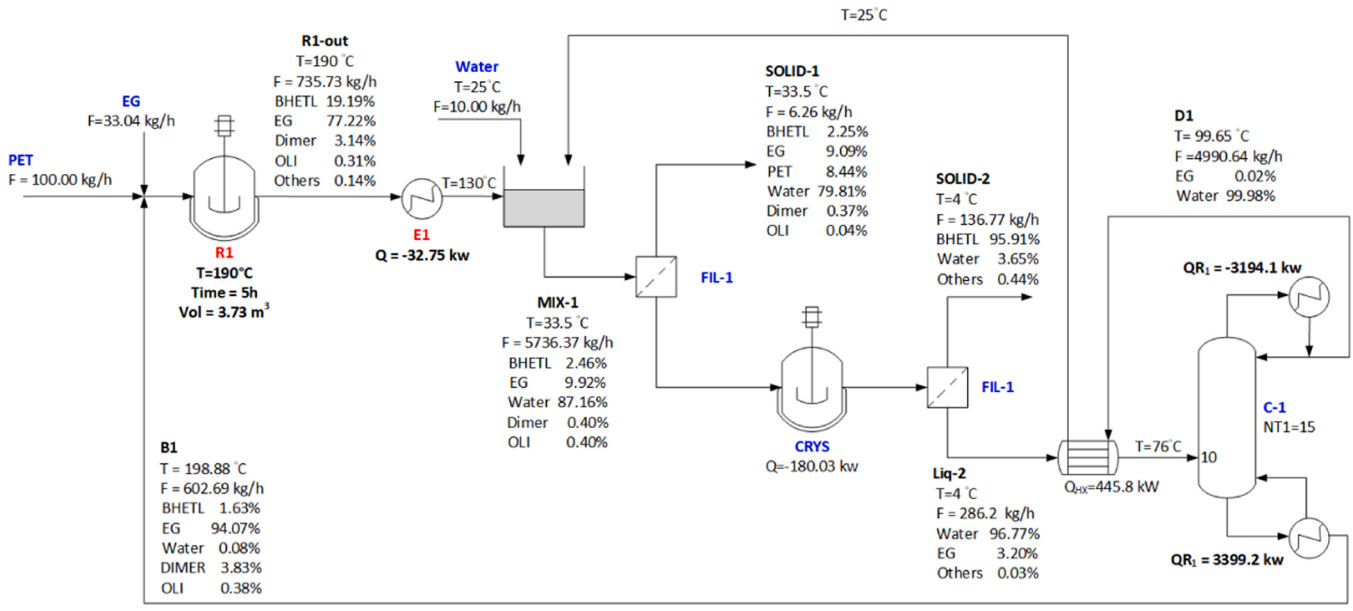

Fig. 10. Proposed flowsheet for the PET glycolysis process.

degradation by the zinc plates in EG. The UV–Vis spectra of the two model compounds in EG in the presence of zinc plates during glycolysis at 190 °C are shown in Fig. 9. The absorption spectra of azobenzene decrease with time, and a new absorption peak appears at shorter wavelengths (Fig. 9a), whereas the absorption spectra of anthraquinone remain unchanged (Fig. 9b). Thus, the zinc plates can degrade azobenzene into smaller molecules in EG at elevated temperatures. Considering these findings and those in the literature regarding azo dye degradation by zero-valent zinc in an acidic aqueous solution [43], a degradation mechanism for azo dyes in EG is proposed, as shown in Scheme 3. The azo groups undergo a reduction reaction to produce the corresponding amines. Based on the different electron acceptors to which zero-valent zinc transfers electrons, two mechanisms are possible. Mechanism 1: Azo dyes are initially absorbed on the surface of zero-valent zinc [43], and zero-valent zinc transfers two electrons to the azo group (–N = N–). Consequently, the azo groups are more vulnerable to the attack of hydrogen sources, including EG or water, and are broken into amines. Mechanism 2: Zero-valent Zn initially transfers electrons to EG or water to produce hydrogen sources [47]. In the presence of hydrogen, the azo groups undergo a series of hydrogenation reactions to be gradually reduced to –HN–NH– and finally to amines ($–NH_2$) [48,49].

4. Process design

With the insights obtained from these experiments, a conceptual design can be developed for the PET glycolysis process. To suitably evaluate the production performance at the process scale, the design basis was scaled up to process 100 kg/h PET. The continuous operation

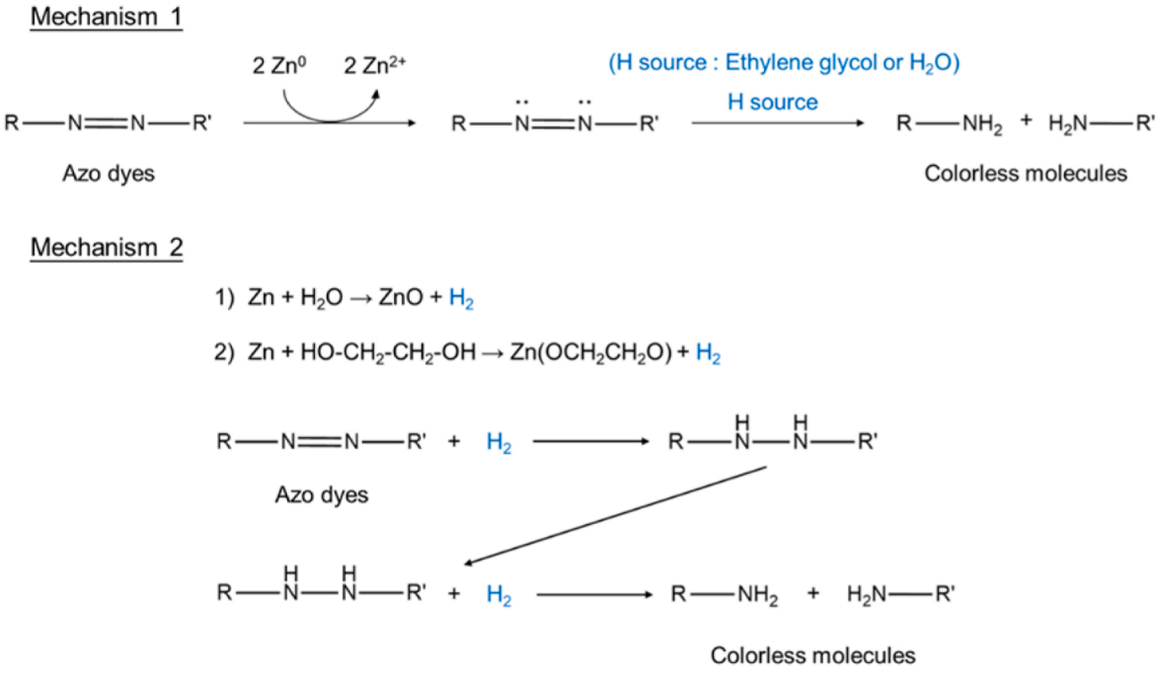

Scheme 3. Proposed mechanism of azo dye degradation over zero-valent zinc.

of each process equipment was considered. Aspen Plus V10 software was used to calculate the mass and energy balance for the process design.

4.1. Components and physical properties

The components included in the simulation were PET (MW: 23829.2 g/mol), oligomer ($C_{62}H_{54}O_{26}$, subsequently denoted as "OLI"; MW: 1215.07 g/mol), dimer ($C_{22}H_{22}O_{10}$; MW: 446.41 g/mol), BHET ($C_{12}H_{14}O_6$; MW: 254.24 g/mol), EG, and water. The first four components were used to describe the progress of the depolymerization. OLI and the dimer were not included in the Aspen database. They were manually defined using the corresponding components, with their structures (i.e., in ". mol" format) available in the NIST database. With reference to the phases, PET was modeled as a solid, whereas the others were fluids. In addition, a crystallization step was introduced to separate BHET from a mixture of EG and water in the proposed process. Hence, two components were used to represent BHET: one for the solid phase ($BHET_S$) and the other for the liquid phase ($BHET_L$).

Many scalar or temperature-dependent properties are required for performing mass and energy balance calculations. For fluidic components, the required scalar components include critical properties (i.e., T_C, P_C, Z_C, V_C), acentric factor, Gibbs energy (ΔG_{form}), and enthalpy of formation (ΔH_{form}). The required temperature-dependent properties are ideal gas heat capacity (CP_{IG}), enthalpy of vaporization (ΔH_{vap}), and vapor pressure (P_{vap}). Moreover, the density, heat capacity, and enthalpy of formation of the solid component are necessary. In this study, most of the pure component properties of the built-in components are readily available from the software. Missing data were estimated using the built-in group-contribution method. For the OLI and dimer, all required properties were estimated using the group-contribution method. All the properties (or the parameters used for calculating the properties) employed in this study are summarized in Table 1S–6S.

The NRTL model was selected for simulating the mixture properties. The binary interaction pairs are presented in Table 7S. In this study, only built-in data are available for the EG/water pair. The remaining pairs were estimated using the UNIFAC method. The structure of OLI cannot be divided into pre-defined functional groups. This hinders the estimation using the UNIFAC method for the binary parameters between OLI and the remaining components. However, OLI is only present in a small amount, and its interaction with the other components can be reasonably neglected.

4.2. Reaction kinetics

In the simulation, the reactions are expressed as Eqs. 10 and 12, respectively. Three steps are primarily considered: depolymerization of PET to oligomers, oligomers to dimers, and dimers to BHET. The final step is assumed to be reversible [3].

$$PET + 20EG \xrightarrow{r_1} 20.632 oligomer \tag{10}$$

$$oligomer + 2EG \xrightarrow{r_2} 3dimer \tag{11}$$

$$dimer + EG \leftrightarrow^{r_3/r_{-3}} 2BHET \tag{12}$$

The individual reaction rates are set as follows: With excess EG, the depolymerization of PET to BHET is considered a pseudo-first-order reaction. The formation of BHET from the dimer and EG is a first-order reaction with a reaction order of 0.5 for the dimer, and 0.5 for EG. Furthermore, the reverse reaction, from BHET to the dimer and EG, is a second-order reaction [50]. The rate expressions are given in Eqs. 13–16, in kmol/kg-cat/s. The concentrations and activation energies are given in kmol/m^3, and in kJ/mol, respectively.

$$r_1 = 4.877 \times 10^{17} e^{-189700/RT} C_{PET} \tag{13}$$

$$r_2 = 3.462 \times 10^{16} e^{-185000/RT} C_{OLI} \tag{14}$$

$$r_3 = 3.173 \times 10^{14} e^{-184000/RT} C_{dimer}^{0.5} C_{EG}^{0.5} \tag{15}$$

$$r_{-3} = 1.248 \times 10^{14} e^{-183000/RT} C_{BHET}^{2} \tag{16}$$

4.3. Process development

The proposed process flowsheet is illustrated in Fig. 10. Initially, 100 kg/h of PET, 33.04 kg/h of fresh EG, and 602.69 kg/h of the recycled EG (~94.07 wt%) are mixed and sent to the depolymerization reactor (**R-1**). The reactor is designed under the optimal conditions obtained from the experiment, particularly, a temperature of 190 °C and residence time of 5 h. Catalyst loading inside the reactor is maintained at 200 kg. The catalyst-to-PET ratio is maintained at 0.4:1, as the total mass holdup of the reactor is 500 kg of PET feed (100 kg/h × 5 h). The reactor is modeled using a built-in RCSTR module. To maintain the reaction at the desired temperature, heat removal of 100.2 kW around the reactor is required. The simulated PET conversion is 99.47%.

After the reaction, the effluent stream is cooled to 130 °C. OLI and the dimer tend to solidify at low temperatures. Hence, cooling the effluent stream to a low temperature is unfavorable. Subsequently, 5000 kg/h of water (25 °C) is added to the solution. This precipitates the unreacted PET. This step is modeled using a mixer (**MIX-1**) and filter unit (**FIL-1**). For **FIL-1**, 0.1% of the solution is assumed to appear at the solid outlet.

The solution from **FIL-1** is sent to a crystallizer (**CRYS**) operated at 4 °C to separate BHET as solids. The solubility of BHET in water, as obtained from the literature (Fig. 14 S), is used to simulate the **CRYS** [51]. The generated solid is separated using a different filter (**FIL-2**). Similar to the setting for **FIL-1**, 0.1% of solution is assumed to flow out with the solid stream. OLI and the dimer are still dissolved in the EG/water solution after crystallization and filtration.

Finally, the EG/water solution is separated through distillation (**C-1**). The targets of separation are set to obtain water of 99.98 wt% purity at the distillate and to recover 99.8% EG from the bottom. **C-1** has 15 theoretical trays (i.e., $NT_1 = 15$), with the feed entering the tenth tray (i.e., $NF_1 = 10$). Herein, NT1 and NF1 were optimized by minimizing the reboiler duty required for the targeted separation, following a sequential iteration search. The results are provided in Fig. 15 S. QR_1 decreases with an increase in NF_1. However, the decrease is diminished upon increasing NT_1 from 15 to 20. Hence, NT_1 is set to 15, and NF_1 is set to 10 to obtain the lowest QR_1. Before entering **C-1**, the feed solution is preheated by exchanging heat (**HX**) with the distillate stream to help conserve energy.

The heavier components (i.e., BHET, OLI, and dimer) entering the feed solution are still dissolved in the bottom stream of **C-1**. Hence, further purification of the stream necessitates the energy-intensive evaporation of EG. In addition, the separated heavier components provide no economic benefit to this process. Consequently, recycling these heavier components in the reactor along with EG is a more practical solution. With this arrangement, the BHET yield can be further enhanced.

Another finding from the simulation is that separating EG and water is energy-intensive. Hence, further studies on the possibility of decreasing the amount of EG used in the reaction or water used for washing are highly recommended.

5. Conclusions

In this study, a PET glycolysis system was developed for producing BHET monomers. Centimeter-sized zinc plates derived from waste batteries were used as the catalysts. When soaked in EG, the zinc plates were found to be highly active toward PET glycolysis, owing to the enhanced contact resulting from the formation of Zn-glycolate and ZnO

during the reaction. Considering PET:EG = 1:6 (wt. basis) and PET: catalyst = 1:0.4 (wt. basis), the optimal PET conversion and yield of BHET were obtained at 89.7% and 77.7%, respectively, at a temperature of 190 °C and residence time of 5 h. Good performance was retained in five runs of the catalyst reusability tests. In addition to depolymerization, the potential for decolorizing PET waste using this reaction system was revealed. Finally, the PET glycolysis process after scaling-up was conceptually designed. Separating EG and water via distillation was found to be the most energy-intensive step. Further improvements can be realized if the challenges associated with the solvent amount and energy requirement are experimentally investigated.

CRediT authorship contribution statement

Yu-Wen Chiao: Conceptualization, Investigation, Data curation, Formal analysis, Visualization, Writing – original draft. **Weisheng Liao:** Conceptualization, Investigation, Data curation, Formal analysis, Writing – review & editing. **Philip Anggo Krisbiantoro:** Investigation, Data curation, Formal analysis, Writing – review & editing. **Bor-Yih Yu:** Formal analysis, Conceptualization, Writing – review & editing. **Kevin C.-W. Wu:** Conceptualization, Formal analysis, Investigation, Project administration, Writing – review & editing, Supervision.

Declaration of Competing Interest

The authors declare that they have no known competing financial interests or personal relationships that could have appeared to influence the work reported in this paper.

Acknowledgments

The authors are grateful to the National Science and Technology Council (NSTC), Taiwan (111-2124-M-002-021, 111-2628-E-002-008, and 111-2221-E-182-001-MY2), and National Taiwan University (NTU), Taiwan (111L894304) for their funding support.

Appendix A. Supporting information

Supplementary data associated with this article can be found in the online version at doi:10.1016/j.apcatb.2022.122302.

References

[1] M. Ghaemy, K. Mossaddegh, Depolymerisation of poly (ethylene terephthalate) fibre wastes using ethylene glycol, Polym. Degrad. Stab. 90 (2005) 570–576.
[2] S. Baliga, W.T. Wong, Depolymerization of poly (ethylene terephthalate) recycled from post-consumer soft-drink bottles, J. Polym. Sci. Part A 1 Polym. Chem. 27 (1989) 2071–2082.
[3] R. López-Fonseca, I. Duque-Ingunza, B. de Rivas, L. Flores-Giraldo, J.I. Gutiérrez-Ortiz, Kinetics of catalytic glycolysis of PET wastes with sodium carbonate, Chem. Eng. J. 168 (2011) 312–320.
[4] C. Jehanno, M.M. Pérez-Madrigal, J. Demarteau, H. Sardon, A.P. Dove, Organocatalysis for depolymerisation, Polym. Chem. 10 (2019) 172–186.
[5] I. Cano, C. Martin, J.A. Fernandes, R.W. Lodge, J. Dupont, F.A. Casado-Carmona, R. Lucena, S. Cardenas, V. Sans, I. de Pedro, Paramagnetic ionic liquid-coated SiO_2@ Fe_3O_4 nanoparticles—The next generation of magnetically recoverable nanocatalysts applied in the glycolysis of PET, Appl. Catal. B Environ. 260 (2020), 118110.
[6] Q. Wang, X. Yao, Y. Geng, Q. Zhou, X. Lu, S. Zhang, Deep eutectic solvents as highly active catalysts for the fast and mild glycolysis of poly(ethylene terephthalate)(PET), Green Chem. 17 (2015) 2473–2479.
[7] J.-T. Du, Q. Sun, X.-F. Zeng, D. Wang, J.-X. Wang, J.-F. Chen, ZnO nanodispersion as pseudohomogeneous catalyst for alcoholysis of polyethylene terephthalate, Chem. Eng. Sci. 220 (2020), 115642.
[8] L.-X. Yun, H. Wu, Z.-G. Shen, J.-W. Fu, J.-X. Wang, Ultrasmall CeO_2 nanoparticles with rich oxygen defects as novel catalysts for efficient glycolysis of polyethylene terephthalate, ACS Sustain. Chem. Eng. (2022).
[9] Q. Suo, J. Zi, Z. Bai, S. Qi, The glycolysis of poly (ethylene terephthalate) promoted by metal organic framework (MOF) catalysts, Catal. Lett. 147 (2017) 240–252.
[10] R.-X. Yang, Y.-T. Bieh, C.H. Chen, C.-Y. Hsu, Y. Kato, H. Yamamoto, C.-K. Tsung, K. C.-W. Wu, Heterogeneous metal azolate framework-6 (MAF-6) catalysts with high zinc density for enhanced polyethylene terephthalate (PET) conversion, ACS Sustain. Chem. Eng. 9 (2021) 6541–6550.
[11] F. Chen, G. Wang, W. Li, F. Yang, Glycolysis of poly (ethylene terephthalate) over Mg–Al mixed oxides catalysts derived from hydrotalcites, Ind. Eng. Chem. Res. 52 (2013) 565–571.
[12] P.A. Krisbiantoro, Y.-W. Chiao, W. Liao, J.-P. Sun, D. Tsutsumi, H. Yamamoto, Y. Kamiya, K.C.-W. Wu, Catalytic glycolysis of polyethylene terephthalate (PET) by solvent-free mechanochemically synthesized MFe_2O_4 (M= Co, Ni, Cu and Zn) spinel, Chem. Eng. J. 450 (2022), 137926.
[13] M.J. Akhtar, M. Ahamed, S. Kumar, M.M. Khan, J. Ahmad, S.A. Alrokayan, Zinc oxide nanoparticles selectively induce apoptosis in human cancer cells through reactive oxygen species, Int. J. Nanomed. 7 (2012) 845.
[14] S. Fakhari, M. Jamzad, H. Kabiri Fard, Green synthesis of zinc oxide nanoparticles: a comparison, Green Chem. Lett. Rev. 12 (2019) 19–24.
[15] N.T. Mai, T.T. Thuy, D.M. Mott, S. Maenosono, Chemical synthesis of blue-emitting metallic zinc nano-hexagons, CrystEngComm 15 (2013) 6606–6610.
[16] M.D.L. Balela, C.M.O. Pelicano, Z. Lockman, In situ mixed potential study of the growth of zinc oxide hierarchical nanostructures by wet oxidation of zinc foil, J. Mater. Sci. 52 (2017) 2319–2328.
[17] H. Umar, D. Kavaz, N. Rizaner, Biosynthesis of zinc oxide nanoparticles using Albizia lebbeck stem bark, and evaluation of its antimicrobial, antioxidant, and cytotoxic activities on human breast cancer cell lines, Int. J. Nanomed. 14 (2019) 87.
[18] Y. Chen, P. Schneider, A. Erbe, Investigation of native oxide growth on zinc in different atmospheres by spectroscopic ellipsometry, Phys. Status Solidi A Mater. Sci. 209 (2012) 846–853.
[19] T.L. Barr, S. Seal, Nature of the use of adventitious carbon as a binding energy standard, J. Vac. Sci. Technol. A Vac. Surf. Films 13 (1995) 1239–1246.
[20] G. Greczynski, L. Hultman, C 1s peak of adventitious carbon aligns to the vacuum level: dire consequences for material's bonding assignment by photoelectron spectroscopy, ChemPhysChem 18 (2017) 1507–1512.
[21] E. Diler, B. Lescop, S. Rioual, G.N. Vien, D. Thierry, B. Rouvellou, Initial formation of corrosion products on pure zinc and $MgZn_2$ examinated by XPS, Corros. Sci. 79 (2014) 83–88.
[22] R. López-Fonseca, I. Duque-Ingunza, B. De Rivas, S. Arnaiz, J. Gutiérrez-Ortiz, Chemical recycling of post-consumer PET wastes by glycolysis in the presence of metal salts, Polym. Degrad. Stab. 95 (2010) 1022–1028.
[23] M.E. Viana, A. Riul, G.M. Carvalho, A.F. Rubira, E.C. Muniz, Chemical recycling of PET by catalyzed glycolysis: kinetics of the heterogeneous reaction, Chem. Eng. J. 173 (2011) 210–219.
[24] F. Pardal, G. Tersac, Kinetics of poly (ethylene terephthalate) glycolysis by diethylene glycol. I. Evolution of liquid and solid phases, Polym. Degrad. Stab. 91 (2006) 2840–2847.
[25] F. Chen, Q. Zhou, R. Bu, F. Yang, W. Li, Kinetics of poly (ethylene terephthalate) fiber glycolysis in ethylene glycol, Fibers Polym. 16 (2015) 1213–1219.
[26] A. Al-Sabagh, F. Yehia, A. Eissa, M. Moustafa, G. Eshaq, A. Rabie, A. ElMetwally, Cu-and Zn-acetate-containing ionic liquids as catalysts for the glycolysis of poly (ethylene terephthalate), Polym. Degrad. Stab. 110 (2014) 364–377.
[27] A.M. Al-Sabagh, F.Z. Yehia, A.-M.M. Eissa, M.E. Moustafa, G. Eshaq, A.-R.M. Rabie, A.E. ElMetwally, Glycolysis of poly (ethylene terephthalate) catalyzed by the Lewis base ionic liquid [Bmim][OAc], Ind. Eng. Chem. Res. 53 (2014) 18443–18451.
[28] B.-Z. Wan, C.-Y. Kao, W.-H. Cheng, Kinetics of depolymerization of poly (ethylene terephthalate) in a potassium hydroxide solution, Ind. Eng. Chem. Res. 40 (2001) 509–514.
[29] J. Campanelli, M. Kamal, D. Cooper, Kinetics of glycolysis of poly (ethylene terephthalate) melts, J. Appl. Polym. Sci. 54 (1994) 1731–1740.
[30] A. Goje, S. Mishra, Chemical kinetics, simulation, and thermodynamics of glycolytic depolymerization of poly (ethylene terephthalate) waste with catalyst optimization for recycling of value added monomeric products, Macromol. Mater. Eng. 288 (2003) 326–336.
[31] K. Takase, H. Nishizawa, K. Imamura, A. Onda, K. Yanagisawa, S. Yin, Synthesis of novel layered zinc glycolate and exchange of ethylene glycol with manganese acetate complex, Bull. Chem. Soc. Jpn. 91 (2018) 1546–1552.
[32] P. Srinivasan, B. Subramanian, Y. Djaoued, J. Robichaud, T. Sharma, R. Bruning, Facile synthesis of mesoporous nanocrystalline ZnO bipyramids and spheres: characterization, and photocatalytic activity, Mater. Chem. Phys. 155 (2015) 162–170.
[33] J. Das, I.R. Evans, D. Khushalani, Zinc glycolate: a precursor to ZnO, Inorg. Chem. 48 (2009) 3508–3510.
[34] K. Ravindranath, R.A. Mashelkar, Polyethylene terephthalate—I. Chemistry, thermodynamics and transport properties, Chem. Eng. Sci. 41 (1986) 2197–2214.
[35] S.M. Biros, B.M. Bridgewater, A. Villeges-Estrada, J.M. Tanski, G. Parkin, Antimony ethylene glycolate and catecholate compounds: structural characterization of polyesterification catalysts, Inorg. Chem. 41 (2002) 4051–4057.
[36] D. Berg, K. Schaefer, A. Koerner, R. Kaufmann, W. Tillmann, M. Moeller, Reasons for the discoloration of postconsumer poly (ethylene terephthalate) during reprocessing, Macromol. Mater. Eng. 301 (2016) 1454–1467.
[37] S. Maerov, Influence of antimony catalysts with hydroxyethoxy ligands on polyester polymerization, J. Polym. Sci. Polym. Chem 17 (1979) 4033–4040.
[38] C. Li, X. Xie, S. Liang, J. Zhou, Issues and future perspective on zinc metal anode for rechargeable aqueous zinc-ion batteries, Energy & Environmental, Materials 3 (2020) 146–159.
[39] I. Martini, E. Chevallay, C. Heßler, V. Nistor, H. Neupert, V. Fedosseev, M. Taborelli, Surface characterization at CERN of photocathodes for photoinjector applications, 2015.
[40] M. Assebban, C. Gibaja, M. Fickert, I. Torres, E. Weinreich, S. Wolff, R. Gillen, J. Maultzsch, M. Varela, S.T.J. Rong, Unveiling the oxidation behavior of liquid-phase exfoliated antimony nanosheets, 2D Mater. 7 (2020), 025039.

[41] I. Koyuncu, R. Sengur, T. Turken, S. Guclu, M. Pasaoglu, Advances in water treatment by microfiltration, ultrafiltration, and nanofiltration. Advances in membrane technologies for water treatment, Elsevier, 2015, pp. 83–128.
[42] N. Abdullah, M.A. Rahman, M.H.D. Othman, J. Jaafar, A.F. Ismail, Membranes and Membrane Processes: Fundamentals, Current Trends and Future Developments on (Bio-) Membranes, Elsevier, 2018, pp. 45–70.
[43] J. Guo, D. Jiang, Y. Wu, P. Zhou, Y. Lan, Degradation of methyl orange by Zn (0) assisted with silica gel, J. Hazard. Mater. 194 (2011) 290–296.
[44] R.J. Chudgar, Azo dyes, Kirk-Othmer Encyclopedia of Chemical Technology, 2000.
[45] S. Benkhaya, S.M′. Rabet, A. El Harfi, A review on classifications, recent synthesis and applications of textile dyes, Inorg. Chem. Commun. 115 (2020).
[46] A. Gürses, M. Açıkyıldız, K. Güneş, M.S. Gürses, Classification of Dye and Pigments, Dyes and Pigments, Springer, 2016, pp. 31–45.
[47] A. Steinfeld, Solar hydrogen production via a two-step water-splitting thermochemical cycle based on Zn/ZnO redox reactions, Int. J. Hydrog. Energy 27 (2002) 611–619.
[48] W.B. Mbarek, M. Azabou, E. Pineda, N. Fiol, L. Escoda, J. Suñol, M. Khitouni, Rapid degradation of azo-dye using Mn–Al powders produced by ball-milling, RSC Adv. 7 (2017) 12620–12628.
[49] Y. Sha, I. Mathew, Q. Cui, M. Clay, F. Gao, X.J. Zhang, Z. Gu, Rapid degradation of azo dye methyl orange using hollow cobalt nanoparticles, Chemosphere 144 (2016) 1530–1535.
[50] A.B. Raheem, A.B. Hassan, Z.Z. Noor, S.B. Samsudin, M. Abd Hamid, A. Bello, O. Oladokun, A.H. Sabeen, A. Shamiri, Process simulation of bis (2-hydroxyethyl) terephthalate and its recovery using two–stage evaporation systems, Chem. Eng. Trans. 63 (2018) 655–660.
[51] F. Pilati, M. Toselli, C. Stramigioli, G. Baldi, M. Capra, M. Osella, G. BavaPilone, Process to prepare bis (2-hydroxyethyl) terephthalate, European Patent EP0723951A1, 31, 1996.